Article

Current Biology

Coherent oscillations across the human brain, spinal cord, and muscle network

Highlights

- Optically pumped magnetometers record brain and spinal cord activity concurrently
- Cervical spinal cord activity is coherent with hand muscle EMG during contraction
- Cortex, cervical cord, and muscle form a bidirectionally coupled 10–35 Hz network
- Spinal and cortical rhythms contribute distinctly to muscle coupling

Authors

Meaghan E. Spedden, Maike Schmidt, George C. O'Neill, ..., Simon F. Farmer, Sven Bestmann, Gareth R. Barnes

Correspondence

m.spedden@ucl.ac.uk

In brief

Spedden et al. use optically pumped magnetometers to record magnetic fields from the human brain and spinal cord at the same time. Coherent 10–35 Hz activity links the sensorimotor cortex, cervical spinal cord, and hand muscle. The coupling is bidirectional, and the cord does not act as a passive relay.

Spedden et al., 2026, Current Biology *36*, 1–12
September 21, 2026 © 2026 The Authors. Published by Elsevier Inc.
https://doi.org/10.1016/j.cub.2026.07.070

CellPress

Please cite this article in press as: Spedden et al., Coherent oscillations across the human brain, spinal cord, and muscle network, Current Biology (2026), https://doi.org/10.1016/j.cub.2026.07.070

Current Biology

CellPress
OPEN ACCESS

Article

Coherent oscillations across the human brain, spinal cord, and muscle network

Meaghan E. Spedden,[1,9,*] Maike Schmidt,[1] George C. O'Neill,[2] Timothy O. West,[1,3,6] Stephanie Mellor,[4,5] Tim M. Tierney,[1] Nicholas A. Alexander,[1] Sahitya Puvvada,[1] Martina F. Callaghan,[1] Simon F. Farmer,[6,7] Sven Bestmann,[1,6,8] and Gareth R. Barnes[1]

[1]Department of Imaging Neuroscience, UCL Queen Square Institute of Neurology, London WC1N 3AR, UK
[2]Department of Neuroscience, Physiology, and Pharmacology, University College London, London WC1E6BT, UK
[3]Department of Bioengineering, Imperial College London, London SW7 2AZ, UK
[4]Spinal Cord Injury Center, Balgrist University Hospital, University of Zurich, 8008 Zurich, Switzerland
[5]Translational Neuromodeling Unit, Institute for Biomedical Engineering, University of Zurich and ETH Zurich, 8032 Zurich, Switzerland
[6]Department for Clinical and Movement Neuroscience, UCL Queen Square Institute of Neurology, University College London, London WC1N 3BG, UK
[7]Department of Clinical Neurology, the National Hospital for Neurology and Neurosurgery, Queen Square, London WC1N 3BG, UK
[8]Centre for Clinical Neuroscience, Hospital Universitario Los Madroños, Brunete 28690, Spain
[9]Lead contact
*Correspondence: m.spedden@ucl.ac.uk
https://doi.org/10.1016/j.cub.2026.07.070

SUMMARY

Voluntary human movement emerges from dynamic interactions between the brain, spinal cord, and sensory afferents. Spinal cord function has proven particularly difficult to study non-invasively in humans due to its deep anatomical location and narrow diameter. As a result, sensorimotor interactions are often studied using cortico-muscular coupling, which captures interactions between brain and muscle but cannot reveal how these signals propagate through the spinal cord. Here, we use concurrent brain and spinal cord imaging with optically pumped magnetometers (OPMs) and electromyography (EMG) to test whether endogenous synchronization within the human sensorimotor system can be detected and characterized non-invasively across cortical, spinal, and muscular levels. Participants (n = 9) performed a sustained isometric hand contraction while we recorded cortical and spinal cord magnetic fields using OPMs and hand muscle activity using EMG, and we compared rhythmic activity propagating through the cortico-spinal-muscular loop with the state at rest. We show that the spinal contribution to cortico-muscular coupling manifests as coherent 10–35 Hz activity linking the contralateral sensorimotor cortex, cervical spinal cord, and muscle. This synchronization forms a distributed, bidirectionally interacting network with physiologically plausible temporal delays. The spatial organization of this activity accords with known sensorimotor anatomy, localizing to cervical segments appropriate for upper-limb control. Our results provide the first direct, non-invasive magnetic field evidence in humans of coherent brain and spinal cord oscillations and demonstrate the feasibility of concurrent, spatiotemporally resolved imaging of the central nervous system to open new avenues for studying human sensorimotor physiology.

INTRODUCTION

Interactions between the brain motor output, the spinal cord, muscle activity, and sensory afferent activity shape the neural control of voluntary movement.[1–3] The spinal cord integrates the activity of afferents with descending motor commands to precisely fine-tune the activation of motor neurons, which provide the final common pathway for transmitting neural activity to the muscle.[4–6] Hence, the spinal cord serves an integrative function critical for natural movement.[2,7] To date, the neurophysiological function of the spinal cord has proven particularly challenging to study in humans, in part due to methodological challenges associated with concurrent spatiotemporal imaging of brain and spinal cord neural activity. This difficulty arises from the spinal cord's small diameter, its deep location within the vertebral canal, and the influence of physiological motion such as cerebrospinal fluid pulsation.[8,9]

The feasibility of non-invasive spinal cord imaging has already been demonstrated using cryogenic magnetospinography (MSG), which detects weak magnetic fields arising from spinal cord neural activity using SQUID sensors. Using this approach, the propagation of neural signals along the spinal cord can be tracked with millisecond temporal resolution, and reconstruction of current flow yields patterns consistent with known sensory pathway physiology.[10–14] However, the system requires cryogenic cooling with liquid helium, the sensor array covers only a limited region of the spinal cord, and participants must remain still with their cord positioned close to the fixed array. Surface electrode-based approaches have also demonstrated the feasibility of non-invasive spinal cord recording, capturing both

This is an open access article under the CC BY license (http://creativecommons.org/licenses/by/4.0/).

Please cite this article in press as: Spedden et al., Coherent oscillations across the human brain, spinal cord, and muscle network, Current Biology (2026), https://doi.org/10.1016/j.cub.2026.07.070

evoked responses and sensorimotor network dynamics.[15–17] However, the spatial resolution of electrode-based methods is limited due to the complexity of predicting the scalp-potential difference rather than the magnetic field due to an electrical source.[18]

A new generation of magnetic sensors, termed optically pumped magnetometers (OPMs), offers considerable flexibility in sensor array construction, which allows us to study the spatio-temporal dynamics of the human nervous system during natural movement.[19,20] OPMs are small ($\sim 12 \times 17 \times 24$ mm), lightweight sensors that can be flexibly placed very near to the body (<10 mm distance).[21–24] This makes it feasible to construct custom arrays covering the head, neck, and back to record brain and spinal cord activity simultaneously. Critically, an OPM-based system for concurrent brain (magnetoencephalography [MEG]) and spinal cord imaging (MSG) has the potential to provide a direct yet non-invasive spatial and temporal window into spinal cord activity and its interactions with the brain and muscles. While OPM-based imaging offers theoretically superior spatial resolution, surface electrode approaches retain practical advantages in terms of cost, portability, and ease of clinical deployment, making the two methods complementary.[15,16,25]

The development of this methodology has important implications for understanding basic motor control as well as the pathophysiology of disorders affecting brain-spinal cord interactions such as stroke, Parkinson's disease, and tremor. We recently introduced a magneto-spino-encephalography (MSEG) approach and demonstrated that we can measure evoked responses at expected latencies from the spinal cord and brain concurrently, using peripheral nerve stimulation.[26]

Building on this work, here we use MSEG to assess the spatio-temporal dynamics of interactions between the brain, spinal cord, and muscle as a basis for voluntary motor behavior. In the sensorimotor system, a large body of research has focused on cortico-muscular coherence, which comprises a phase and amplitude coupling between neural activity in the sensorimotor cortex (electroencephalogram [EEG] or MEG) and muscle activity (electromyography [EMG]).[27] This coherence emerges during low-level tonic contraction of distal muscles and exhibits a characteristic beta-band peak.[28–31] It is also expressed as a common drive to individual motor neurons within and between muscles.[29,31] High-density surface EMG decomposition has further demonstrated that cortico-muscular coherence reflects common synaptic input to the motor neuron pool, reconstructed from cumulative motor unit spike trains as an estimate of neural drive to muscle. Together, these findings indicate that rhythmic activity is transmitted between cortex and muscle via spinal pathways. There is strong evidence supporting a descending cortico-spinal component.[32,33] However, cortico-muscular coherence can also be influenced by sensory feedback within the sensorimotor loop.[34]

Consequently, although cortico-muscular coherence demonstrates that rhythmic cortical activity reaches the motor neuron pool via spinal cord pathways, our understanding of spinal dynamics during movement has largely relied on indirect inference from muscle activity. While high-density EMG provides detailed insight into the output stage of spinal processing, i.e., the motor neuron pool, it cannot directly resolve activity within the broader spinal circuitry, including interneuronal networks and ascending sensory pathways. Thus, it remains unclear whether this coherent signal is directly and non-invasively observable at the level of spinal population activity and whether its spectral and temporal structure is preserved or transformed by spinal cord network dynamics. Notably, invasive recordings in non-human primates have demonstrated coherence between spinal cord local field potentials (LFPs) and muscle activity during precision grip,[35,36] suggesting that the spinal cord population expresses structured oscillatory dynamics.

Here, we directly and non-invasively investigate rhythmic activity in the human spinal cord (10–35 Hz) and its interactions with brain and muscle activity. Using a custom-built array of OPMs to record concurrently from the brain and spinal cord, together with surface EMG during a simple voluntary contraction, we test whether beta-band sensorimotor synchronization can be detected and characterized across cortical, spinal, and muscular levels and whether its spectral and temporal structure reflects anatomically grounded coupling within the sensorimotor pathway. We hypothesized that beta-band activity in the contralateral sensorimotor cortex, cervical spinal cord, and muscle would exhibit significant coherence during contraction relative to rest.

RESULTS

We used OPMs to map rhythmic interactions across cortical, spinal, and muscular levels of the sensorimotor pathway during voluntary contraction. Triaxial OPMs were mounted in a custom scanner-cast positioned over the scalp, neck, chest, and back, and surface EMG was recorded from the right abductor pollicis brevis (APB), a thumb muscle innervated via the C8-T1 segments of the cervical cord (Figures 1A and 1B). Participants lay supine and alternated between two-min blocks of weak, sustained right thumb contraction and 2-min blocks of rest. Coherence was computed between rectified EMG and source-reconstructed cortical and spinal cord activity. Of the nine participants included in the analyses, all provided usable spinal cord data, whereas seven also provided usable brain data. Results are therefore reported for $n = 9$ or $n = 7$ depending on the signals involved (STAR Methods). The scanner-cast was constructed using the anatomy of participant 1, giving the most precise sensor-to-anatomy correspondence in that participant. Results for participant 1 are therefore presented alongside group-level results throughout.

Muscle activity is coherent with the contralateral sensorimotor cortex

We first identified cortical sources exhibiting coherence with right APB activity as a marker of cortico-muscular coupling. Sources were reconstructed using dynamic imaging of coherent sources (DICS) beamforming, a spatial filtering approach that maps coherence between each candidate source location and a reference signal, here, the EMG.

Figure 2 shows brain regions exhibiting significantly greater coherence with right APB activity during contraction relative to rest for participant 1 and at the group level (Figures 2A and 2B, respectively). Participant 1 exhibited a clear and spatially focal region of significant coherence in the left sensorimotor cortex, consistent with the expected physiology and connectivity. Control analyses using unrectified EMG performed on data from

Please cite this article in press as: Spedden et al., Coherent oscillations across the human brain, spinal cord, and muscle network, Current Biology (2026), https://doi.org/10.1016/j.cub.2026.07.070

CellPress
OPEN ACCESS

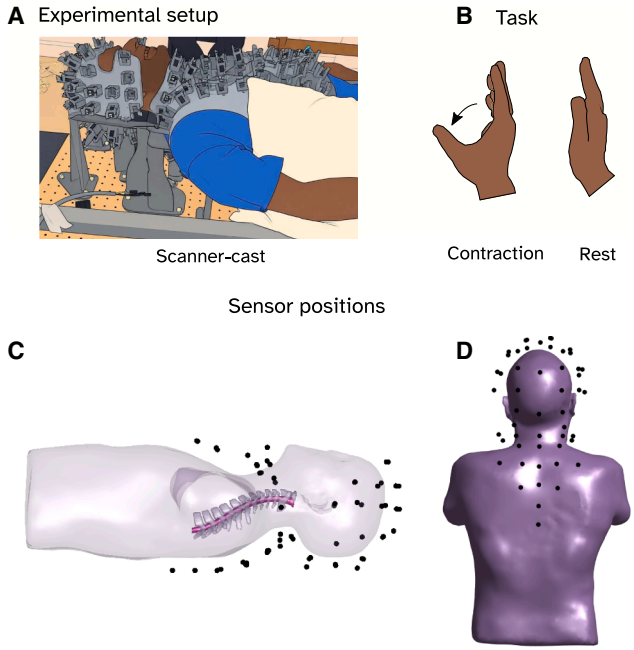

Figure 1. Experimental setup

(A) Participants lay supine on a bed in the magnetically shielded room in a custom-built scanner-cast holding sensors over the scalp, neck, chest, and back. The cast was populated with 64 triaxial OPMs.

(B) Participants performed a weak, sustained thumb contraction interspersed with periods of rest. EMG was recorded from the right abductor pollicis brevis.

(C and D) Sensor positions relative to participant 1's anatomy.

participant 1 produced a broader, bilaterally distributed pattern of cortical coherence less consistent with contralateral motor cortex engagement during unilateral hand contraction (Figures S1A and S1B).

Significance was assessed within each participant against a permutation-derived null distribution. Across participants, six out of seven displayed significant coherence with the EMG in at least one brain source. We treated each participant as an independent replication and summarized consistency across the cohort using Bayesian prevalence inference,[37] which estimates the proportion of the population expected to show a true effect given the number of significant participants and the false-positive rate of the single-participant test. The estimated population prevalence was 0.85, with a 95% highest posterior density interval (HPDI) of 0.50–0.99. Prevalence mapping (Figure 2B), which gives the fraction of participants showing a significant effect at each source location, further revealed that the left sensorimotor cortex showed the highest spatial concentration of such effects.

Coherence was estimated over the full duration of the contraction period. Coherence did not differ significantly between the early and late portions of the contraction period (Figure S2), indicating that this did not obscure a transient peak in coupling strength.

Muscle activity is coherent with the cervical spinal cord

Having established the presence of cortico-muscular coherence, we next asked whether this rhythmic activity could also be detected in the spinal cord.

Figure 3 shows spinal cord sources exhibiting significant coherence with right APB activity in the 10–35 Hz frequency band. In participant 1, we observed significant coherence across a broad cranial-caudal region with the maximum around C5-C6 (Figure 3A). Spinal cord segmentation for anatomical reference is shown in Figure S3A. Control analyses using unrectified EMG performed on data from participant 1 yielded no significant spinal cord-EMG coherence (Figure S1C).

Across the nine participants with spinal cord data, seven showed significant spinal cord-EMG coherence in at least one spinal cord location. Population prevalence was estimated at 0.77 (95% HPDI: 0.45–0.95).

At the group level, prevalence mapping (Figure 3B) showed that this coherence was most consistently expressed around the C7 vertebra.[16,38] Figure S3B illustrates the spatial distribution of peak coherence locations for each participant. This distribution covers cervical segments involved in upper-limb innervation, suggesting we can detect physiologically meaningful spinal cord engagement during voluntary contraction.

We next examined the dominant source orientation at the spinal location exhibiting the maximal coherence difference

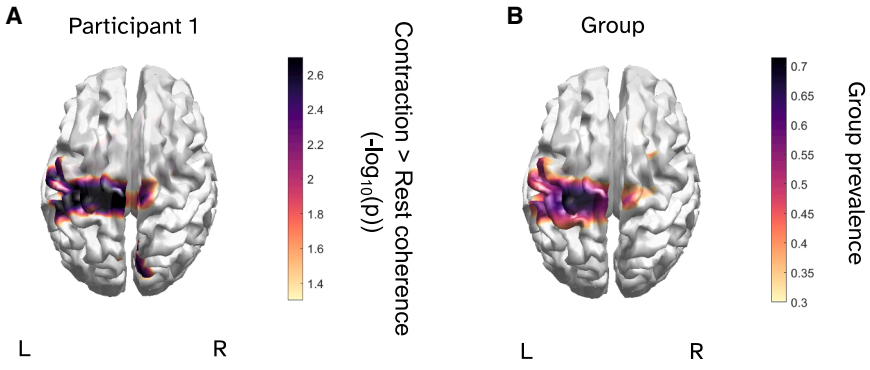

Figure 2. Brain sources coherent with right thumb EMG

(A) Sources showing significant coherence (10–35 Hz) with right thumb EMG for participant 1, displayed as −log10(FWE-corrected p values) from permutation testing (thresholded at $p < 0.05$). Higher values indicate stronger evidence for coherence during contraction relative to rest (one-tailed test). Coherence is localized to the left sensorimotor cortex (MNI −46, −16, 45).

(B) Group-level prevalence map showing the proportion of participants exhibiting significant coherence at each brain source. For each participant, coherence was first thresholded for statistical significance ($p < 0.05$, FWE-corrected), and the prevalence map was then thresholded at 0.3 to highlight regions consistently engaged across participants. The left sensorimotor cortex showed the highest group-level prevalence (MNI −57, −32, 31). Significant sources were determined via permutation testing ($n = 500$), with the significance threshold defined as the 95th percentile of the maximal values across permutations.

See also Figures S1 and S2.

Please cite this article in press as: Spedden et al., Coherent oscillations across the human brain, spinal cord, and muscle network, Current Biology (2026), https://doi.org/10.1016/j.cub.2026.07.070

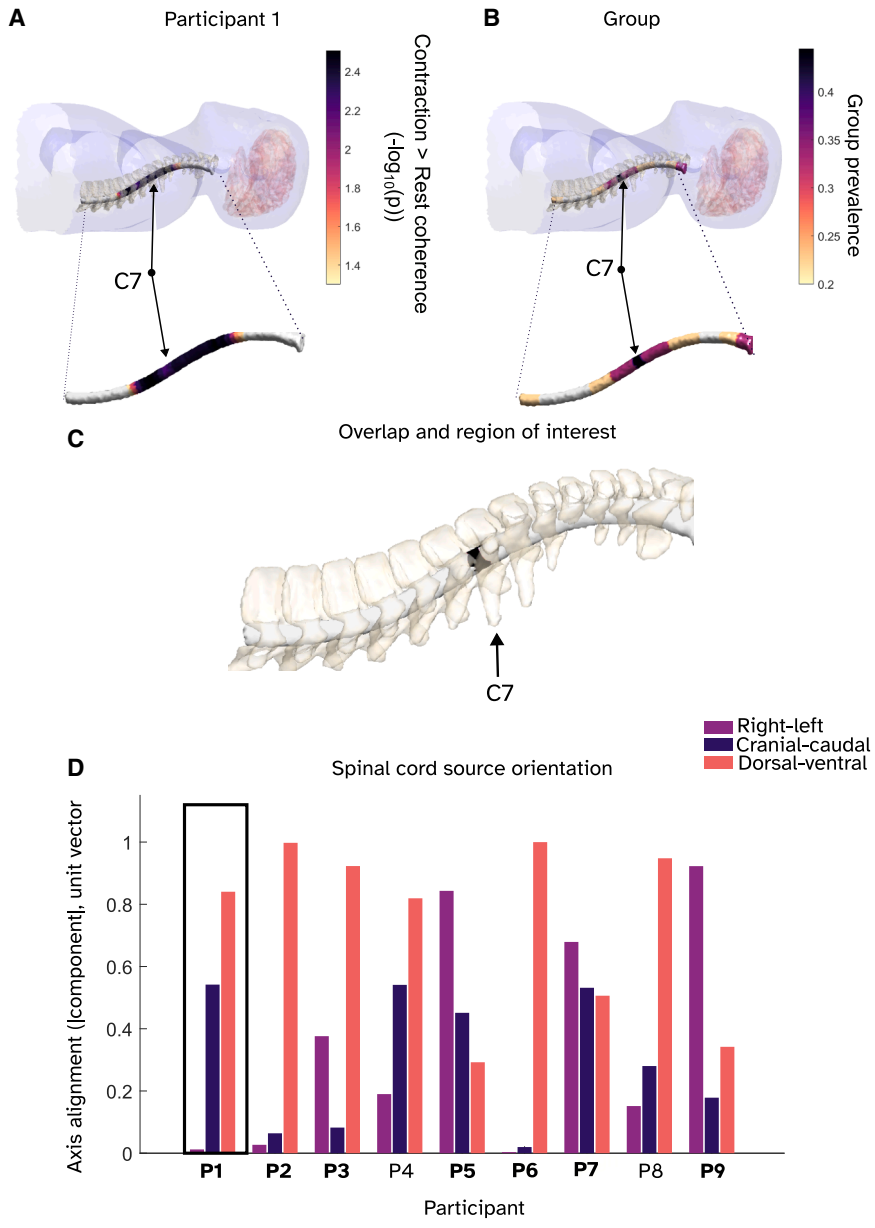

Figure 3. Spinal cord sources coherent with right thumb EMG

(A) Spinal cord sources showing significant coherence with right thumb EMG for participant 1 in the 10–35 Hz frequency band, displayed as −log10(FWE-corrected p values) from permutation testing (thresholded at $p < 0.05$). Higher values indicate stronger evidence for coherence during contraction relative to rest (one-tailed test). For visualization, the empirical permutation distribution at each source was fit with a smooth curve to obtain a continuous −log10(p) mapping. Significant coherence spans a relatively broad cranial-caudal region of the cervical spinal cord.

(B) Group-level prevalence map showing the proportion of participants exhibiting significant coherence at each spinal source. For each participant, coherence was first thresholded for statistical significance ($p < 0.05$, FWE-corrected), and the prevalence map was then thresholded at 0.2 to highlight regions engaged across participants. Significant sources were determined via permutation testing ($n = 500$), with the significance threshold defined as the 95th percentile of the maximal values across permutations.

(C) Region of peak prevalence relative to C7.

(D) Bars represent the degree of alignment along each axis for the spinal cord source showing maximal coherence with EMG for each participant. Participant 1 is highlighted (black box). A predominant dorsal-ventral orientation was observed in participant 1 and in six of nine participants overall. Bold font indicates participants showing statistically significant spinal cord-EMG coherence.

See also Figures S1, S3, and S4.

(contraction-rest). For participant 1, the predominant orientation was aligned along the dorsal-ventral axis (Figure 3D). This orientation was observed in six of nine participants, indicating consistent alignment of the identified spinal cord generator across individuals.

To determine whether the spinal cord source location and orientation identified by the spinal cord-EMG DICS analysis reflected a genuine task-related effect rather than a bias of the source reconstruction procedure, we examined the spatial and orientational distribution of peak coherence differences obtained under permutation for participant 1.

As shown in Figure 4A, permutation maxima were distributed broadly across the cranio-caudal extent of the source space, with minor boundary effects at the edges of the finite source grid. The observed peak does not coincide with a location that is preferentially selected under the null, supporting the spatial specificity of the identified source. Figure 4B shows the normalized orientation components at the peak coherence location for participant 1 alongside the permutation distribution. The observed peak exhibits a dominant dorsal-ventral orientation. However, permutation maxima show a similarly dominant dorsal-ventral component, indicating a reconstruction bias toward this orientation that limits orientational specificity claims at the individual level. In some participants, we observed right-left or mixed dominance, a pattern inconsistent with uniform reconstruction bias, suggesting that source orientation reflects individual differences in the dominant spinal generator rather than a systematic artifact of the reconstruction procedure.

To further assess the robustness of the identified spinal source to potential sources of variability in the forward model, we examined the sensitivity of the Biot-Savart leadfields to sensor array displacements spanning the range of inter-participant positional variability observed in the current dataset (STAR Methods). As shown in Figure S4A, R^2 between lead fields computed at the original and displaced sensor positions remained above 0.95 across the full cranio-caudal extent of the source space for displacements

Please cite this article in press as: Spedden et al., Coherent oscillations across the human brain, spinal cord, and muscle network, Current Biology (2026), https://doi.org/10.1016/j.cub.2026.07.070

CellPress
OPEN ACCESS

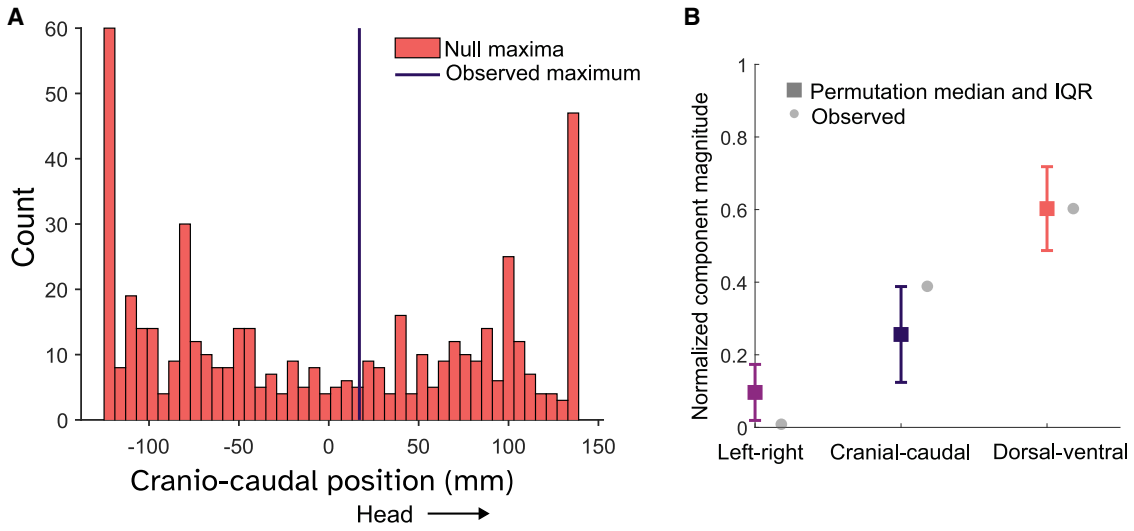

Figure 4. Spatial specificity and source orientation of spinal cord coherence

(A) Spatial specificity check for participant 1. Histogram showing the cranio-caudal location of the maximal coherence difference (contraction-rest) across 500 label permutations. Permutation maxima show clustering at the two boundary points of the source space, reflecting edge effects due to its finite extent. Between these boundary peaks, maxima are broadly distributed, with no preferential selection of the observed peak location (vertical blue line).

(B) Orientation of spinal cord source at peak location for participant 1. Colored squares show the median ± IQR of each normalized orientation component (left-right, cranio-caudal, and dorsal-ventral) across permutation peak locations. Gray dots show the observed values. Note that observed data and null permutations show similar dorsal-ventral dominance.

spanning the observed range of inter-participant variability, and the spatial profile of spinal cord-EMG coherence was largely preserved under a representative displacement (Figure S4B). Together with the permutation analyses described above, these findings support the robustness of the identified spinal source to both statistical and geometric sources of uncertainty.

Network coupling is bidirectional with anatomically ordered delays

Having established coherence between the cortex and muscle and the spinal cord and muscle, we next asked whether the brain and spinal cord signals were coherent with each other. To do this, we extracted a single representative time series (a "virtual electrode") from each of two regions of interest: a sensorimotor cortical region defined from the brain-EMG coherence prevalence map and the spinal cord region showing the largest contiguous cluster of coherence with EMG across participants (Figures 5A and 5B). Figure 5C shows peak brain-spinal cord coherence for each participant during contraction, expressed as a multiple of that participant's own 95% upper confidence limit, such that values above 1 indicate significant coherence. Four out of seven participants, including participant 1, exhibited

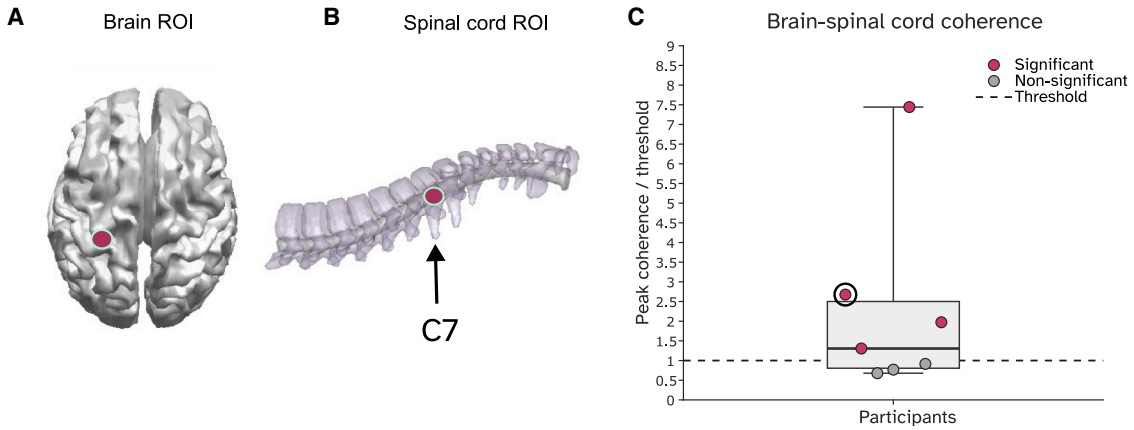

Figure 5. Brain-spinal cord coherence

(A) Location of the brain region of interest used for constructing brain virtual electrodes.

(B) Location of the spinal cord region of interest used to construct spinal cord virtual electrodes.

(C) Peak brain-spinal cord coherence (10–35 Hz) for each participant during contraction, normalized to that participant's own 95% upper confidence limit (dashed line, ratio = 1). The circled point indicates participant 1. The box shows the median and IQR.

Please cite this article in press as: Spedden et al., Coherent oscillations across the human brain, spinal cord, and muscle network, Current Biology (2026), https://doi.org/10.1016/j.cub.2026.07.070

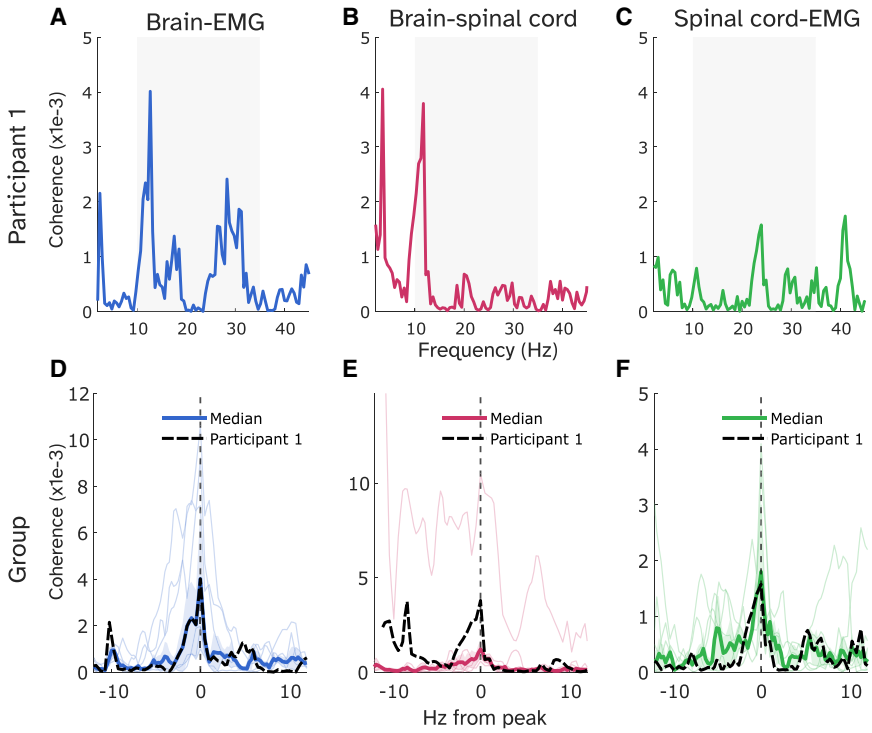

Figure 6. Coherence spectra

(A–C) Coherence spectra for brain-EMG (A), brain-spinal cord (B), and spinal cord-EMG (C) signal pairs for participant 1, derived from brain and spinal cord virtual electrodes.

(D–F) Individual coherence spectra for all participants for each signal pair (faint lines). Spectra are aligned to each participant's dominant peak frequency within the frequency band of interest (10–35 Hz), centered at 0 Hz, to account for inter-individual variability in peak frequency. The solid line shows the median across participants. The dotted black trace shows participant 1.

See also Figures S5 and S6 and Table S1.

significant coherence between the brain and spinal cord signals. Population prevalence was estimated at 0.55 (95% HPDI: 0.22–0.84).

We then characterized the dynamics of interactions within the identified network using brain and spinal cord virtual electrodes together with the EMG signal. Figure 6 shows coherence spectra as a function of frequency for participant 1 (A–C) and individual traces for all participants (D–F). Peak coherence frequency varied across participants and signal pairs (Figures S5E and S6; median peak frequencies: brain-EMG 20 Hz [MAD 5.37 Hz], brain-spinal cord 19 Hz [MAD 7.32 Hz], and spinal cord-EMG 24 Hz [MAD 5.37 Hz]). Brain-spinal cord coherence in participant 1 peaked at the lower end of the analysis band (12 Hz), notably lower than the group median for this signal pair. To account for inter-individual variability in peak coherence frequency, individual traces are aligned to each participant's dominant peak frequency within the beta band (10–35 Hz). Peak coherence for each participant and signal pair is reported in Table S1.

To assess whether the same oscillation tracks linearly through the cortico-spinal network, we examined whether brain-EMG coherence was reduced when partialling out the spinal cord signal (STAR Methods; Figure S5). This reduced brain-EMG coherence in three of seven participants, but the percentage coherence reduction did not differ significantly from zero (Wilcoxon signed-rank test, signed rank = 16.0, $p = 0.812$). As a complementary test of the same question, we asked whether coherence peaked at the same frequency across the three signal pairs, reasoning that a single oscillation propagating unchanged through the network should produce a common peak frequency throughout. Peak coherence frequencies differed significantly between the brain-EMG and cord-EMG pairs (paired t test, $t(6) = -2.94$, $p = 0.026$) but not for the remaining two comparisons (brain-cord and brain-EMG, $t(6) = -0.75$, $p = 0.484$; cord-EMG and brain-cord, $t(6) = -1.18$, $p = 0.283$). Together, these findings suggest that the spinal cord is not acting as a passive relay that forwards the signal unchanged.

Directed coherence was computed for each signal pair to quantify ascending and descending coupling within the 10–35-Hz band (Figure 7A), which provides a frequency-resolved estimate of coupling direction without assuming a parametric model. For participant 1, as well as across participants, we observed contributions in both directions along the brain-spinal cord-muscle pathway, indicating bidirectional sensorimotor interactions. As a robustness check, we additionally computed the phase slope index (PSI), which infers directionality from the consistency of the phase difference across frequencies. This indicated similarly bidirectional flow of information (Figure S7).

Temporal delays were estimated from the peak of the normalized cumulant density (ρ) (Figure 7B), a time-domain measure equivalent to a whitened cross-correlation, whose peak identifies the lag at which activity in one signal best predicts the other. The ordering of latencies was consistent with the anatomy of the pathway: the longest delays were observed for brain-EMG interactions (participant 1, 42 ms; median for group [$n = 7$], 39 ms and MAD, 5 ms), with shorter delays for brain-spinal cord coupling (participant 1, 10 ms; median for group, 8 ms and MAD, 2 ms) and spinal cord-EMG coupling (group median, 12 ms and MAD, 9 ms). Brain-EMG delays are consistent with peak cortico-muscular coherence delays reported previously.[39,40] The group median spinal cord-EMG delay of 12 ms is consistent with expected peripheral conduction times from the cervical cord to the hand. The corresponding value for participant 1 (4 ms) was shorter, which may reflect the difficulty of obtaining precise conduction delay estimates from coherence-based measures.

Neural power changes do not account for coherence effects

As a control analysis, we tested whether the observed coherence effects could be explained by differences in neural spectral power between rest and contraction. We compared 10–35 Hz

Please cite this article in press as: Spedden et al., Coherent oscillations across the human brain, spinal cord, and muscle network, Current Biology (2026), https://doi.org/10.1016/j.cub.2026.07.070

CellPress
OPEN ACCESS

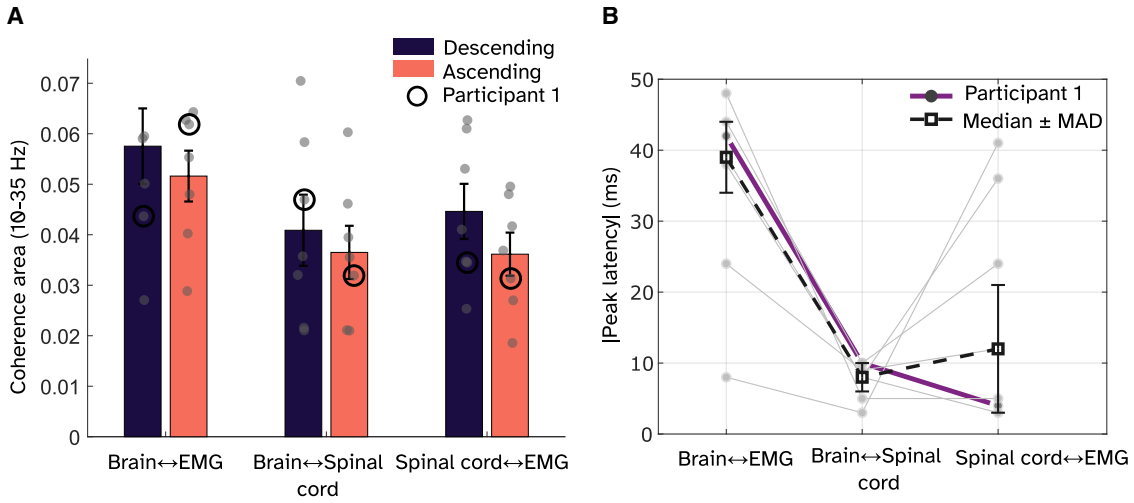

Figure 7. Directionality and temporal dynamics of coherence between brain, spinal cord, and muscle during contraction

(A) Area under the curve for directed coherence spectra (10–35 Hz) across participants. Coherence was observed in both directions along the brain-spinal cord-muscle pathway (i.e., descending and ascending), consistent with bidirectional sensorimotor interactions. Values for participant 1 are highlighted with a circle. Error bars show SEM.

(B) Absolute latencies of the normalized cumulant density indicating the lag at which signals are coupled. Peaks were identified within a physiologically plausible window (±50 ms), excluding zero lags (±2 ms) to reduce shared-noise effects. Participant 1's results are highlighted with a solid purple line. Gray lines show individual participants.

See also Figure S7.

power extracted from the spinal cord and sensorimotor cortex virtual electrodes across conditions.

Participant 1 showed a significant decrease in spinal cord spectral power during contraction relative to rest (paired t test across 1-s segments, $n = 523$; $t(522) = -19.08$, $p < 0.001$), while no such difference was observed for the brain virtual electrode ($t(522) = -0.33$, $p = 0.739$).

At the group level, we did not detect any differences (paired t test across participants, $n = 7$; spinal cord, $t(6) = -0.682$, $p = 0.520$; brain, $t(6) = -1.415$, $p = 0.207$). When we examined the periodic component of the spectrum in the frequency band of interest, we similarly found no significant difference between rest and contraction conditions for either the brain or spinal cord signals (brain, $t(6) = -1.01$, $p = 0.35$; spinal cord, $t(6) = -0.390$, $p = 0.71$).

DISCUSSION

We demonstrate that rhythmic interactions can be detected and characterized non-invasively across cortical, cervical spinal, and muscular levels using OPM-based recordings. This activity forms a distributed, anatomically structured, and temporally organized network linking the contralateral sensorimotor cortex, cervical spinal cord, and muscle during voluntary contraction.

Cortico-muscular coherence

We found significant cortico-muscular coherence with the right APB muscle localized to the left sensorimotor cortex. This effect was detectable at the single-participant level and consistently across participants, highlighting the sensitivity of OPM-based recordings. These findings are consistent with a large body of work showing that sensorimotor cortical and distal muscle activity are coupled at beta frequencies during maintained contraction using the coherence metric.[28–30,33]

This cortico-muscular functional connectivity suggests that rhythmic activity is transmitted through the spinal cord, where it can impact and be impacted by spinal cord neurons.[36] To our knowledge, this is the first demonstration of cortico-muscular coherence using OPMs. Replicating this well-established effect provides a validation of the approach and establishes a foundation for detecting the transmission of this signal through the spinal cord.

Spinal cord-muscle coherence

Significant spinal cord-EMG coherence was observed across a relatively broad cranio-caudal region for participant 1, spanning cervical segments consistent with upper-limb innervation. The cervical spinal cord at C8-T1 is the primary site of both the motoneurons innervating the intrinsic hand muscles and the afferent input from those muscles via the median nerve. The spatial distribution of significant coherence in our data is therefore anatomically consistent with engagement of the motor and sensory spinal circuits mediating voluntary thumb contraction.

Prior work using cryogenic spinal cord recordings has identified multiple potential signal sources, including synchronized synaptic currents in spinal gray matter and dorsal root entry potentials.[10] Given our use of low-frequency coherence (10–35 Hz) as the primary metric, the spinal cord signal identified here is more likely to reflect rhythmic synchronized synaptic input than action potentials. The dominant dorsal-ventral source orientation observed in most participants is anatomically consistent with current flow from the dorsal horn, which receives afferent sensory input, toward the ventral horn, where the motor neuron pools innervating the upper limb are located. While permutation analysis indicated

Please cite this article in press as: Spedden et al., Coherent oscillations across the human brain, spinal cord, and muscle network, Current Biology (2026), https://doi.org/10.1016/j.cub.2026.07.070

that the reconstruction procedure has some tendency toward dorsal-ventral orientations at peak locations, the presence of alternative dominant orientations in a subset of participants suggests this finding is not solely attributable to reconstruction bias.

Across participants, the location of significant coherence along the spinal cord source space varied. This variability is likely due to differences in sensor positioning and scanner-cast fit across individuals, as well as the use of a common anatomical reference model constructed from a single participant and applied to all, rather than reflecting differences in segmental organization of sensory or motor pathways. Notably, significant spino-muscular coherence was detected in seven out of nine participants, indicating that the effect is robust at the individual level despite reduced spatial specificity.

Spino-muscular coherence may arise from oscillatory input via descending pathways or sensory afferents. Primate studies have demonstrated cervical LFP-EMG coherence during precision grip tasks within a frequency range overlapping that examined here.[36] Subsequent work has replicated spino-muscular coherence effects and provided evidence for both afferent and efferent contributions.[35]

To our knowledge, this is the first demonstration of coherence between non-invasively recorded spinal cord field activity and muscle activity in humans. This approach is highly complementary to existing non-invasive methods, including high-density EMG for resolving motoneuronal discharge patterns.[33,41,42] Together, these techniques offer the potential to bridge cortical, spinal, and muscular levels of the sensorimotor system within a unified experimental framework.

The spinal signals observed here likely reflect a mixture of descending cortico-spinal drive, propriospinal and interneuronal network activity, afferent input, and motoneuronal population dynamics. Although the relative contributions of these circuits cannot be resolved with the present data, the ability to detect their aggregate rhythmic interactions non-invasively provides a new experimental framework in which these contributions can be systematically manipulated and quantified.

Taken together, our findings are consistent with animal work[35,36] and suggest that spinal cord contributions to sensorimotor loops can be captured using the present approach. Although future work will be needed to resolve the contributions of specific circuits, the present approach opens a new avenue for studying spinal cord function and dysfunction in disorders such as spinal cord injury, cervical myelopathy, and motor neuron disease.

Cortico-spinal cord coherence

Significant coherence between the brain and spinal cord virtual electrodes was observed in four of seven participants, a lower prevalence than for either brain-EMG or spinal cord-EMG coherence. This likely reflects the greater technical challenge of estimating coherence between two reconstructed neural sources, both of which have a lower signal-to-noise ratio than EMG recordings. Additionally, EMG-referenced coherence measures are anchored to the final output stage of a specific motor pool, providing a more specific reference signal. Despite these challenges, significant cortico-spinal coherence was detected in the majority of participants, demonstrating that rhythmic interactions between the cortex and spinal cord can be resolved non-invasively.

Oscillatory coupling between motor cortical LFPs and the spinal cord has been previously demonstrated in monkeys during sustained upper-limb contraction in frequency bands overlapping the one examined here.[35] In humans, non-invasive electrospinography (ESG) has recently emerged as a complementary approach to MSG for studying spinal cord networks.[16] To date, ESG studies have shown they can detect evoked spinal cord responses as well as high-frequency oscillations associated with somatosensory transmission.[16,17] Two recent studies have additionally reported EEG-ESG movement-related coherence in the beta band around C5-C7.[15,25]

Together, these findings place our results in close agreement with existing animal and human work. Importantly, we extend this literature by demonstrating coherence using magnetic field measurements and by capturing coherent oscillatory activity across the entire neuroaxis, spanning cortex, spinal cord, and muscle.

Network dynamics: Directionality and temporal dynamics

Directed coherence and cumulant density analyses revealed bidirectional interactions between the cortex, spinal cord, and muscle. This is consistent with previous work showing the influence of changes in sensory feedback on cortico-muscular coherence.[43,44] Estimated delays clustered within physiologically plausible conduction windows. The longest latencies were observed for brain-EMG interactions (median: 39 ms), broadly consistent with peak cortico-muscular coherence delays reported previously.[39,40] Shorter delays were observed for brain-spinal cord coupling (median: 8 ms) and spinal cord-EMG coupling (median: 12 ms), consistent with the shorter distances involved in these sub-segments of the pathway.[45] It is important to note, however, that interpreting cumulant peaks as simple conduction delays is not straightforward, as the timing relationship between signals during sustained contraction may not always resolve to a single meaningful latency.[30]

To examine whether these pairwise interactions reflect a single oscillation propagating serially through the network, we assessed partial coherence and compared peak coherence frequencies across signal pairs. When variance attributable to the spinal cord signal was removed, cortico-muscular coherence was reduced in three of seven participants, suggesting that the spinal cord may contribute to the shared coupling between cortical and muscular activity in at least a subset of individuals. However, this effect was not observed consistently across participants.

Further evidence against a simple serial propagation model came from the frequency analysis. Paired *t* tests indicated that the peak frequencies of brain-EMG and spinal cord-EMG coherence differed significantly, whereas no significant differences were observed between the other signal-pair combinations. If a single oscillatory process were propagated linearly from the cortex through the spinal cord to the muscle, similar peak frequencies would be expected across all coherence measures. Instead, these findings suggest that the spinal cord participates in the network with a degree of oscillatory independence, consistent with active processing and transformation of rhythmic signals rather than passive relay.

This interpretation is consistent with observations in non-human primates. Oya and colleagues reported that spino-muscular

Please cite this article in press as: Spedden et al., Coherent oscillations across the human brain, spinal cord, and muscle network, Current Biology (2026), https://doi.org/10.1016/j.cub.2026.07.070

and cortico-muscular coherence peaked at distinct frequencies in the beta band and were associated with different sensorimotor feedback loops engaged during dynamic and static phases of a precision grip task.[35] Their findings suggest that spinal and cortical circuits contribute to motor control through partially separable oscillatory mechanisms rather than through the transmission of a single shared oscillation. The present results extend this perspective to non-invasive human recordings and support the view that spinal networks make an active contribution to the generation and shaping of sensorimotor rhythms.

Methodological considerations and limitations

The preprocessing pipeline followed established OPM processing procedures where appropriate, incorporating HFC and synthetic gradiometry as developed for brain OPM recordings, together with standard temporal filtering and SSP. While these methods proved effective for detecting spinal coherence, dedicated optimization for spinal cord measurements represents an important direction for future work.

A further consideration is whether the reconstructed spinal coherence could reflect paraspinal muscle activity. Importantly, spinal cord oscillatory power did not increase during contraction, and the observed localization was spatially specific relative to the permutation null distribution. Also, the spinal-cord source space was defined deep within the torso, rather than along superficial posterior tissues where neck and back muscle activity would be expected to dominate. Together, these factors argue against a purely muscular origin of the reconstructed spinal coherence signal.

Respiration induces changes in chest geometry and spinal cord motion that were not explicitly modeled in the forward model. In these analyses, we focused on the cervical spinal cord, which undergoes respiratory displacement on the sub-millimeter level,[46] so that the geometric error introduced into the forward model at the level of our recordings is relatively minimal. In addition, our coherence analysis focused on 10–35 Hz, well above the respiratory frequency (~0.2–0.3 Hz), such that temporal high-pass filtering effectively removed the dominant respiratory contribution to the recorded signals. Furthermore, coherence was estimated from many contraction epochs. Any respiration-driven fluctuations in lead field accuracy would be expected to average out given that respiratory motion has no fixed phase relationship to the task.

This study used a single bipolar electrode pair placed over the target muscle. Future studies would benefit from placing additional EMG electrodes over neighboring muscles to examine relationships with synergists and antagonists and, ideally, from using a high-density EMG grid. High-density surface EMG provides more sensitive detection of cortico-muscular coherence compared with bipolar recordings[33,47] and additionally allows the isolation of single motor unit discharge times. This would enable approaches similar to spike-triggered averaging in which motor unit firing times are used to interrogate coupled spinal cord activity.

We made use of a Biot-Savart law approximation to the forward model (as used in Akaza et al.,[10] Hashimoto et al.,[12] and Adachi and Kawabata[14]). This model is simple but has the advantage that it does not require individual anatomical data and therefore provides a consistent framework applicable across all participants equally. A limitation is that this approach does not incorporate individual variation in spinal cord geometry, tissue conductivities, or sensor-to-cord distances, which may reduce the precision of spatial localization compared with participant-specific anatomical models.[48,49] In Figure S4, we provide a direct comparison between the robustness of this approximation and a more complex forward model to sensor displacement. Future work incorporating individual anatomical models for all participants would further improve spatial precision and allow more precise group-level localization of spinal cord sources.

There could be a concern that a portion of the observed spinal cord coherence is due to occipital cortical rather than spinal-cord sources. We think this is unlikely for a number of reasons: firstly, the spinal-cord source was established through coherence with the EMG, which did not show significant coherence with the occipital lobe (Figure 2). Secondly, one would expect an occipital cortical source to drive the location of peak coherence toward the cranial boundary, i.e., more like our null simulations (Figure 4A) rather than the mid-cervical location observed. Finally, the source reconstructions were derived from a beamformer using a data-covariance matrix spanning all signal channels (covering both brain and cord), so one would expect any zero-lag covariance (due to the same source but imprecise lead fields) to be suppressed.

OPM-based systems give us the flexibility to study the spatiotemporal dynamics of the entire nervous system, which is virtually unprecedented. Interactions between different regions of the CNS and the periphery are at the core of voluntary movement control, and OPM-based systems uniquely allow us to study this functional integration directly and non-invasively. In this work, we kept participants still to minimize interference. As we advance our understanding of spinal cord signals and the associated sources of interference, it will become possible to record activity during larger-scale, more naturalistic movements. This would allow us to investigate, e.g., locomotor-related spinal dynamics, such as central pattern generator activity, and how they are affected in neurological disease. Comparable measurements during movement are already feasible for brain activity using MEG-based approaches,[20,50,51] and extending similar capabilities to the spinal cord will represent an important step toward naturalistic and global imaging of the sensorimotor system.

Conclusion

In this work, we demonstrate that rhythmic sensorimotor interactions can be detected and characterized non-invasively across cortical, cervical spinal, and muscular levels using magnetic field recordings and EMG. This coherent 10–35 Hz activity forms a distributed and temporally structured network with anatomically grounded organization along the human brain-spinal cord-muscle pathway. These findings establish a framework for directly measuring spinal network participation in human sensorimotor coupling and enable spatiotemporally resolved investigation of central nervous system dynamics across the brain-spinal cord-muscle axis.

RESOURCE AVAILABILITY

Lead contact

Further information and requests for resources should be directed to and will be fulfilled by the lead contact, Meaghan E. Spedden (m.spedden@ucl.ac.uk).

Please cite this article in press as: Spedden et al., Coherent oscillations across the human brain, spinal cord, and muscle network, Current Biology (2026), https://doi.org/10.1016/j.cub.2026.07.070

Materials availability

This study did not generate any new, unique reagents.

Data and code availability

- All OPM (magnetoencephalographic and magnetospinographic), electromyographic, and derived data reported in this paper have been deposited at Zenodo and are publicly available as of the date of publication (https://zenodo.org/records/20824565 and https://zenodo.org/records/20824827). DOIs are listed in the key resources table.
- All original analysis code has been deposited at GitHub (https://github.com/meaghanspedden/brainspine-connectivity) and is publicly available as of the date of publication. The DOI is listed in the key resources table.
- Any additional information required to reanalyze the data reported in this paper is available from the lead contact upon request.

ACKNOWLEDGMENTS

M.E.S. and this work were supported by a Wellcome Technology development grant 223736/Z/21/Z. S.M. was funded by an Engineering and Physical Sciences Research Council (EPSRC) Healthcare Impact Partnership grant (EP/V047264/1). G.C.O. was funded by a UKRI Frontier Research Grant (EP/X023060/1). T.M.T. is funded by an ERUK fellowship (FY2101). This research was supported by the Discovery Research Platform for Naturalistic Neuroimaging funded by Wellcome (226793/Z/22/Z) and an MRC equipment grant (MR/X012409/1). S.B. was funded by the Biotechnology and Biological Sciences Research Council (BBSRC; BB/X008614/1) and is supported by The Humane Research Trust (THRT). THRT funds only non-animal research. T.O.W. was supported by the Department for Science, Innovation, and Technology, the Royal Academy of Engineering under the Research Fellowships and the Rosetrees Trust (RAoE\4).

AUTHOR CONTRIBUTIONS

M.E.S., S.B., and G.R.B. devised the project. G.C.O., S.P., M.S., T.O.W., S.M., T.M.T., N.A.A., M.E.S., and G.R.B. wrote software. All authors contributed to the interpretation of the results and to the writing and editing of the manuscript.

DECLARATION OF INTERESTS

The authors declare no competing interests.

DECLARATION OF GENERATIVE AI AND AI-ASSISTED TECHNOLOGIES IN THE WRITING PROCESS

During the preparation of this work, the authors used Claude to assist with manuscript preparation, including editing of text, and with the development of analysis code. After using this tool, the authors carefully reviewed and edited the content as needed and take full responsibility for the content of the publication.

STAR★METHODS

Detailed methods are provided in the online version of this paper and include the following:

- KEY RESOURCES TABLE
- EXPERIMENTAL MODEL AND STUDY PARTICIPANT DETAILS
  - Human participants
- METHOD DETAILS
  - OPM-based recording system
  - EMG recordings
  - Task
  - Data analysis software
  - Preprocessing of OPM and EMG data
  - Co-registration and forward models
  - Source localization of coherent activity
  - Spinal cord source geometry
  - Spatial specificity of the spinal source
  - Virtual electrodes
  - Coherence, directionality, and dynamics
  - Spectral power
  - Forward model sensitivity analysis
  - Boundary element model comparison
  - Partial coherence and peak frequency
- QUANTIFICATION AND STATISTICAL ANALYSIS
  - Single-participant inference
  - Population prevalence inference
  - Reporting of statistical parameters

SUPPLEMENTAL INFORMATION

Supplemental information can be found online at https://doi.org/10.1016/j.cub.2026.07.070.

Received: April 10, 2026
Revised: May 1, 2026
Accepted: July 29, 2026

REFERENCES

1. Nielsen, J.B. (2004). Sensorimotor integration at spinal level as a basis for muscle coordination during voluntary movement in humans. J. Appl. Physiol. (1985) *96*, 1961–1967. https://doi.org/10.1152/japplphysiol.01073.2003.
2. Nielsen, J.B. (2016). Human spinal motor control. Annu. Rev. Neurosci. *39*, 81–101. https://doi.org/10.1146/annurev-neuro-070815-013913.
3. Umeda, T., Isa, T., and Nishimura, Y. (2022). Temporal dynamics of the sensorimotor convergence underlying voluntary limb movement. Proc. Natl. Acad. Sci. USA *119*, e2208353119. https://doi.org/10.1073/pnas.2208353119.
4. Fetz, E.E., Perlmutter, S.I., Prut, Y., Seki, K., and Votaw, S. (2002). Roles of primate spinal interneurons in preparation and execution of voluntary hand movement. Brain Res. Brain Res. Rev. *40*, 53–65. https://doi.org/10.1016/S0165-0173(02)00188-1.
5. Hochman, S. (2007). Spinal cord. Curr. Biol. *17*, R950–R955. https://doi.org/10.1016/j.cub.2007.10.014.
6. Jankowska, E. (1992). Interneuronal relay in spinal pathways from proprioceptors. Prog. Neurobiol. *38*, 335–378. https://doi.org/10.1016/0301-0082(92)90024-9.
7. Bosco, G., and Poppele, R.E. (2001). Proprioception from a spinocerebellar perspective. Physiol. Rev. *81*, 539–568. https://doi.org/10.1152/physrev.2001.81.2.539.
8. Stroman, P.W., Wheeler-Kingshott, C., Bacon, M., Schwab, J.M., Bosma, R., Brooks, J., Cadotte, D., Carlstedt, T., Ciccarelli, O., Cohen-Adad, J., et al. (2014). The current state-of-the-art of spinal cord imaging: methods. NeuroImage *84*, 1070–1081. https://doi.org/10.1016/j.neuroimage.2013.04.124.
9. Spedden, M.E., O'Neill, G.C., Tierney, T.M., West, T.O., Schmidt, M., Mellor, S., Farmer, S.F., Bestmann, S., and Barnes, G.R. (2024). Towards non-invasive imaging through spinal-cord generated magnetic fields. Front. Med. Technol. *6*, 1470970. https://doi.org/10.3389/fmedt.2024.1470970.
10. Akaza, M., Kawabata, S., Ozaki, I., Miyano, Y., Watanabe, T., Adachi, Y., Sekihara, K., Sumi, Y., and Yokota, T. (2021). Noninvasive measurement of sensory action currents in the cervical cord by magnetospinography. Clin. Neurophysiol. *132*, 382–391. https://doi.org/10.1016/j.clinph.2020.11.029.
11. Kawabata, S., Komori, H., Mochida, K., Harunobu, O., and Shinomiya, K. (2002). Visualization of conductive spinal cord activity using a biomagnetometer. Spine *27*, 475–479. https://doi.org/10.1097/00007632-200203010-00007.

Please cite this article in press as: Spedden et al., Coherent oscillations across the human brain, spinal cord, and muscle network, Current Biology (2026), https://doi.org/10.1016/j.cub.2026.07.070

12. Hashimoto, J., Kawabata, S., Sasaki, T., Hoshino, Y., Sekihara, K., Adachi, Y., Watanabe, T., Miyano, Y., Mitani, Y., Sato, S., et al. (2022). Assessment of thoracic spinal cord electrophysiological activity through magnetoneurography. Clin. Neurophysiol. *133*, 39–47. https://doi.org/10.1016/j.clinph.2021.09.023.

13. Sato, T., Adachi, Y., Tomori, M., Ishii, S., Kawabata, S., and Sekihara, K. (2009). Functional imaging of spinal cord electrical activity from its evoked magnetic field. IEEE Trans. Biomed. Eng. *56*, 2452–2460. https://doi.org/10.1109/TBME.2009.2025506.

14. Adachi, Y., and Kawabata, S. (2024). SQUID magnetoneurography: an old-fashioned yet new tool for noninvasive functional imaging of spinal cords and peripheral nerves. Front. Med. Technol. *6*, 1351905. https://doi.org/10.3389/fmedt.2024.1351905.

15. Steele, A.G., Faraji, A.H., and Contreras-Vidal, J.L. (2024). Electrospinography for non-invasively recording spinal sensorimotor networks in humans. J. Neural Eng. *20*. https://doi.org/10.1088/1741-2552/ad1782.

16. Nierula, B., Stephani, T., Bailey, E., Kaptan, M., Pohle, L.G., Horn, U., Mouraux, A., Maess, B., Villringer, A., Curio, G., et al. (2024). A multichannel electrophysiological approach to noninvasively and precisely record human spinal cord activity. PLoS Biol. *22*, e3002828. https://doi.org/10.1371/journal.pbio.3002828.

17. Chander, B.S., Deliano, M., Azañón, E., Büntjen, L., and Stenner, M.P. (2022). Non-invasive recording of high-frequency signals from the human spinal cord. NeuroImage *253*, 119050. https://doi.org/10.1016/j.neuroimage.2022.119050.

18. Baillet, S. (2017). Magnetoencephalography for brain electrophysiology and imaging. Nat. Neurosci. *20*, 327–339. https://doi.org/10.1038/nn.4504.

19. West, T.O., Spedden, M.E., O'Neill, G., Bestmann, S., Barnes, G., Farmer, S.F., Cagnan, and H.. (2025). The cerebellum implements an oscillatory forward model for accurate motor timing. Preprint at bioRxiv. https://doi.org/10.1101/2025.11.11.687835.

20. O'Neill, G.C., Seymour, R.A., Mellor, S., Alexander, N.A., Tierney, T.M., Bernachot, L., Fahimi Hnazaee, M., Spedden, M.E., Timms, R.C., Bush, D., et al. (2025). Combining video telemetry and wearable MEG for naturalistic imaging. Imaging Neurosci. *3*, imag_a_00495. https://doi.org/10.1162/imag_a_00495.

21. Alem, O., Hughes, K.J., Buard, I., Cheung, T.P., Maydew, T., Griesshammer, A., Holloway, K., Park, A., Lechuga, V., Coolidge, C., et al. (2023). An integrated full-head OPM-MEG system based on 128 zero-field sensors. Front. Neurosci. *17*, 1190310. https://doi.org/10.3389/fnins.2023.1190310.

22. Brookes, M.J., Leggett, J., Rea, M., Hill, R.M., Holmes, N., Boto, E., and Bowtell, R. (2022). Magnetoencephalography with optically pumped magnetometers (OPM-MEG): the next generation of functional neuroimaging. Trends Neurosci. *45*, 621–634. https://doi.org/10.1016/j.tins.2022.05.008.

23. Gutteling, T.P., Bonnefond, M., Clausner, T., Daligault, S., Romain, R., Mitryukovskiy, S., Fourcault, W., Josselin, V., Le Prado, M., Palacios-Laloy, A., et al. (2023). A new generation of OPM for high dynamic and large bandwidth MEG: the 4He OPMs-first applications in healthy volunteers. Sensors *23*, 2801. https://doi.org/10.3390/s23052801.

24. Tierney, T.M., Holmes, N., Mellor, S., López, J.D., Roberts, G., Hill, R.M., Boto, E., Leggett, J., Shah, V., Brookes, M.J., et al. (2019). Optically pumped magnetometers: from quantum origins to multi-channel magnetoencephalography. NeuroImage *199*, 598–608. https://doi.org/10.1016/j.neuroimage.2019.05.063.

25. Mehra, P., Bista, S., Metzger, M., Giglia, E.R., Plaitano, S., Nash, L., Domhnaill, E.M., Bede, P., Mathuraman, M., Hardiman, O., et al. (2025). Spinal electrophysiology reveals frequency-specific spatial patterns of neural activity and corticospinal coherence during pincer-grip. Preprint at bioRxiv. https://doi.org/10.1101/2025.11.11.687864.

26. Mardell, L.C., Spedden, M.E., O'Neill, G.C., Tierney, T.M., Timms, R.C., Zich, C., Barnes, G.R., and Bestmann, S. (2024). Concurrent spinal and brain imaging with optically pumped magnetometers. J. Neurosci. Methods *406*, 110131. https://doi.org/10.1016/j.jneumeth.2024.110131.

27. van Wijk, B.C.M., Beek, P.J., and Daffertshofer, A. (2012). Neural synchrony within the motor system: what have we learned so far? Front. Hum. Neurosci. *6*, 252. https://doi.org/10.3389/fnhum.2012.00252.

28. Conway, B.A., Halliday, D.M., Farmer, S.F., Shahani, U., Maas, P., Weir, A.I., and Rosenberg, J.R. (1995). Synchronization between motor cortex and spinal motoneuronal pool during the performance of a maintained motor task in man. J. Physiol. *489*, 917–924. https://doi.org/10.1113/jphysiol.1995.sp021104.

29. Farmer, S.F., Bremner, F.D., Halliday, D.M., Rosenberg, J.R., and Stephens, J.A. (1993). The frequency content of common synaptic inputs to motoneurones studied during voluntary isometric contraction in man. J. Physiol. *470*, 127–155. https://doi.org/10.1113/jphysiol.1993.sp019851.

30. Halliday, D.M., Conway, B.A., Farmer, S.F., and Rosenberg, J.R. (1998). Using electroencephalography to study functional coupling between cortical activity and electromyograms during voluntary contractions in humans. Neurosci. Lett. *241*, 5–8. https://doi.org/10.1016/S0304-3940(97)00964-6.

31. Farmer, S.F. (1998). Rhythmicity, synchronization and binding in human and primate motor systems. J. Physiol. *509*, 3–14. https://doi.org/10.1111/j.1469-7793.1998.003bo.x.

32. Hansen, N.L., and Nielsen, J.B. (2004). The effect of transcranial magnetic stimulation and peripheral nerve stimulation on corticomuscular coherence in humans. J. Physiol. *561*, 295–306. https://doi.org/10.1113/jphysiol.2004.071910.

33. Ibáñez, J., Del Vecchio, A., Rothwell, J.C., Baker, S.N., and Farina, D. (2021). Only the fastest corticospinal fibers contribute to β corticomuscular coherence. J. Neurosci. *41*, 4867–4879. https://doi.org/10.1523/JNEUROSCI.2908-20.2021.

34. Baker, S.N. (2007). Oscillatory interactions between sensorimotor cortex and the periphery. Curr. Opin. Neurobiol. *17*, 649–655. https://doi.org/10.1016/j.conb.2008.01.007.

35. Oya, T., Takei, T., and Seki, K. (2020). Distinct sensorimotor feedback loops for dynamic and static control of primate precision grip. Commun. Biol. *3*, 156. https://doi.org/10.1038/s42003-020-0861-0.

36. Takei, T., and Seki, K. (2008). Spinomuscular coherence in monkeys performing a precision grip task. J. Neurophysiol. *99*, 2012–2020. https://doi.org/10.1152/jn.01181.2007.

37. Ince, R.A., Paton, A.T., Kay, J.W., and Schyns, P.G. (2021). Bayesian inference of population prevalence. eLife *10*, e62461. https://doi.org/10.7554/eLife.62461.

38. Gabrieli, G., Somervail, R., Mouraux, A., Leandri, M., Haggard, P., and Iannetti, G.D. (2025). Electrical Spinal Imaging: A noninvasive, high-resolution approach that enables electrophysiological mapping of the human spinal cord. PLoS Biol. *23*, e3003116. https://doi.org/10.1371/journal.pbio.3003116.

39. Salenius, S., Portin, K., Kajola, M., Salmelin, R., and Hari, R. (1997). Cortical control of human motoneuron firing during isometric contraction. J. Neurophysiol. *77*, 3401–3405. https://doi.org/10.1152/jn.1997.77.6.3401.

40. Gross, J., Tass, P.A., Salenius, S., Hari, R., Freund, H.J., and Schnitzler, A. (2000). Cortico-muscular synchronization during isometric muscle contraction in humans as revealed by magnetoencephalography. J. Physiol. *527*, 623–631. https://doi.org/10.1111/j.1469-7793.2000.00623.x.

41. Dideriksen, J.L., Negro, F., Falla, D., Kristensen, S.R., Mrachacz-Kersting, N., and Farina, D. (2018). Coherence of the surface EMG and common synaptic input to motor neurons. Front. Hum. Neurosci. *12*, 207. https://doi.org/10.3389/fnhum.2018.00207.

42. Graef, C., Pascual Valdunciel, A., Farina, D., Vaidyanathan, R., Tai, Y.F., and Haar, S. (2026). Propagation of beta bursts from the motor cortex to the motor units of multiple upper-limb muscles. J. Neurophysiol. *135*, 97–109. https://doi.org/10.1152/jn.00336.2025.

43. Fisher, R.J., Galea, M.P., Brown, P., and Lemon, R.N. (2002). Digital nerve anaesthesia decreases EMG-EMG coherence in a human precision grip

task. Exp. Brain Res. *145*, 207–214. https://doi.org/10.1007/s00221-002-1113-x.

44. Riddle, C.N., and Baker, S.N. (2005). Manipulation of peripheral neural feedback loops alters human corticomuscular coherence. J. Physiol. *566*, 625–639. https://doi.org/10.1113/jphysiol.2005.089607.
45. Rossini, P.M., Burke, D., Chen, R., Cohen, L.G., Daskalakis, Z., Di Iorio, R., Di Lazzaro, V., Ferreri, F., Fitzgerald, P.B., George, M.S., et al. (2015). Non-invasive electrical and magnetic stimulation of the brain, spinal cord, roots and peripheral nerves: Basic principles and procedures for routine clinical and research application. An updated report from an I.F.C.N. Committee. Clin. Neurophysiol. *126*, 1071–1107. https://doi.org/10.1016/j.clinph.2015.02.001.
46. Winklhofer, S., Schoth, F., Stolzmann, P., Krings, T., Mull, M., Wiesmann, M., and Stracke, C.P. (2014). Spinal cord motion: influence of respiration and cardiac cycle. RoFo *186*, 1016–1021. https://doi.org/10.1055/s-0034-1366429.
47. Piitulainen, H., Botter, A., Bourguignon, M., Jousmäki, V., and Hari, R. (2015). Spatial variability in cortex-muscle coherence investigated with magnetoencephalography and high-density surface electromyography. J. Neurophysiol. *114*, 2843–2853. https://doi.org/10.1152/jn.00574.2015.
48. O'Neill, G.C., Spedden, M.E., Schmidt, M., Mellor, S., Stenroos, M., and Barnes, G.R. (2025). Volume conductor models for magnetospinography. Sci. Rep. *15*, 26258. https://doi.org/10.1038/s41598-025-10770-z.
49. Schmidt, M., Barnes, G., O'Neill, G., and Spedden, M. (2026). Forward modelling in magnetospinography. In Proceedings of the Workshop Biosignale, J. Vorwerk, M. Handler, and D. Baumgarten, eds. (Innsbruck University Press).
50. Seymour, R.A., Alexander, N., Mellor, S., O'Neill, G.C., Tierney, T.M., Barnes, G.R., and Maguire, E.A. (2021). Using OPMs to measure neural activity in standing, mobile participants. NeuroImage *244*, 118604. https://doi.org/10.1016/j.neuroimage.2021.118604.
51. Spedden, M.E., O'Neill, G.C., West, T.O., Tierney, T.M., Mellor, S., Alexander, N.A., Seymour, R., Lundbye-Jensen, J., Nielsen, J.B., Farmer, S.F., et al. (2025). Using wearable MEG to study the neural control of human stepping. Sensors (Basel) *25*, 4160. https://doi.org/10.3390/s25134160.
52. Tierney, T.M., Alexander, N.A., Ashburner, J., Avila, N.L., Balbastre, Y., Barnes, G., Bezsudnova, Y., Brudfors, M., Eckstein, K., Flandin, G., et al. (2025). SPM 25: Open source neuroimaging analysis software. JOSS *10*, 8103. https://doi.org/10.21105/joss.08103.
53. Oostenveld, R., Fries, P., Maris, E., and Schoffelen, J.M. (2011). FieldTrip: open source software for advanced analysis of MEG, EEG, and invasive electrophysiological data. Comput. Intell. Neurosci. *2011*, 156869. https://doi.org/10.1155/2011/156869.
54. Halliday, D.M. (2015). Nonparametric directionality measures for time series and point process data. J. Integr. Neurosci. *14*, 253–277. https://doi.org/10.1142/S0219635215300127.
55. Warszawer, Y., Molinier, N., Valošek, J., Benveniste, P.-L., Bédard, S., Shirbint, E., Mohamed, F.B., Tsagkas, C., Kolind, S., and Lynd, L., et al. (2025). TotalSpineSeg: robust spine segmentation with landmark-based labeling in MRI. https://doi.org/10.13140/RG.2.2.31318.56649.
56. Van Oosterom, A., and Oostendorp, T.F. (2004). ECGSIM: an interactive tool for studying the genesis of QRST waveforms. Heart *90*, 165–168. https://doi.org/10.1136/hrt.2003.014662.
57. Rea, P. (2016). Essential Clinically Applied Anatomy of the Peripheral Nervous System in the Head and Neck (Elsevier), pp. 131–183.
58. Beck, M.M., Spedden, M.E., Dietz, M.J., Karabanov, A.N., Christensen, M.S., and Lundbye-Jensen, J. (2021). Cortical signatures of precision grip force control in children, adolescents, and adults. eLife *10*, e61018. https://doi.org/10.7554/eLife.61018.
59. Spedden, M.E., Jensen, P., Terkildsen, C.U., Jensen, N.J., Halliday, D.M., Lundbye-Jensen, J., Nielsen, J.B., and Geertsen, S.S. (2019). The development of functional and directed corticomuscular connectivity during tonic ankle muscle contraction across childhood and adolescence. NeuroImage *191*, 350–360. https://doi.org/10.1016/j.neuroimage.2019.02.054.
60. Tierney, T.M., Alexander, N., Mellor, S., Holmes, N., Seymour, R., O'Neill, G.C., Maguire, E.A., and Barnes, G.R. (2021). Modelling optically pumped magnetometer interference in MEG as a spatially homogeneous magnetic field. NeuroImage *244*, 118484. https://doi.org/10.1016/j.neuroimage.2021.118484.
61. Uusitalo, M.A., and Ilmoniemi, R.J. (1997). Signal-space projection method for separating MEG or EEG into components. Med. Biol. Eng. Comput. *35*, 135–140. https://doi.org/10.1007/BF02534144.
62. Fife, A.A., Vrba, J., Robinson, S.E., Anderson, G., Betts, K., Burbank, M.B., Cheyne, D., Cheung, T., Govorkov, S., Haid, G., et al. (1999). Synthetic gradiometer systems for MEG. IEEE Trans. Appl. Supercond. *9*, 4063–4068. https://doi.org/10.1109/77.783919.
63. Halliday, D.M., and Farmer, S.F. (2010). On the need for rectification of surface EMG. J. Neurophysiol. *103*, 3547. https://doi.org/10.1152/jn.00222.2010.
64. Isensee, F., Jaeger, P.F., Kohl, S.A.A., Petersen, J., and Maier-Hein, K.H. (2021). nnU-Net: a self-configuring method for deep learning-based biomedical image segmentation. Nat. Methods *18*, 203–211. https://doi.org/10.1038/s41592-020-01008-z.
65. Nolte, G. (2003). The magnetic lead field theorem in the quasi-static approximation and its use for magnetoencephalography forward calculation in realistic volume conductors. Phys. Med. Biol. *48*, 3637–3652. https://doi.org/10.1088/0031-9155/48/22/002.
66. Gross, J., Kujala, J., Hämäläinen, M., Timmermann, L., Schnitzler, A., and Salmelin, R. (2001). Dynamic imaging of coherent sources: studying neural interactions in the human brain. Proc. Natl. Acad. Sci. USA *98*, 694–699. https://doi.org/10.1073/pnas.98.2.694.
67. West, T.O., Halliday, D.M., Bressler, S.L., Farmer, S.F., and Litvak, V. (2020). Measuring directed functional connectivity using non-parametric directionality analysis: validation and comparison with non-parametric Granger causality. NeuroImage *218*, 116796. https://doi.org/10.1016/j.neuroimage.2020.116796.
68. Thomson, D.J. (1982). Spectrum estimation and harmonic analysis. Proc. IEEE *70*, 1055–1096. https://doi.org/10.1109/PROC.1982.12433.
69. Halliday, D.M., Rosenberg, J.R., Amjad, A.M., Breeze, P., Conway, B.A., and Farmer, S.F. (1995). A framework for the analysis of mixed time series/point process data—Theory and application to the study of physiological tremor, single motor unit discharges and electromyograms. Prog. Biophys. Mol. Biol. *64*, 237–278. https://doi.org/10.1016/S0079-6107(96)00009-0.
70. Nolte, G., Ziehe, A., Nikulin, V.V., Schlögl, A., Krämer, N., Brismar, T., and Müller, K.R. (2008). Robustly estimating the flow direction of information in complex physical systems. Phys. Rev. Lett. *100*, 234101. https://doi.org/10.1103/PhysRevLett.100.234101.
71. Donoghue, T., Haller, M., Peterson, E.J., Varma, P., Sebastian, P., Gao, R., Noto, T., Lara, A.H., Wallis, J.D., Knight, R.T., et al. (2020). Parameterizing neural power spectra into periodic and aperiodic components. Nat. Neurosci. *23*, 1655–1665. https://doi.org/10.1038/s41593-020-00744-x.
72. Maris, E., Schoffelen, J.M., and Fries, P. (2007). Nonparametric statistical testing of coherence differences. J. Neurosci. Methods *163*, 161–175. https://doi.org/10.1016/j.jneumeth.2007.02.011.
73. Fries, P., and Maris, E. (2022). What to do if N is two? J. Cogn. Neurosci. *34*, 1114–1118. https://doi.org/10.1162/jocn_a_01857.

Please cite this article in press as: Spedden et al., Coherent oscillations across the human brain, spinal cord, and muscle network, Current Biology (2026), https://doi.org/10.1016/j.cub.2026.07.070

CellPress
OPEN ACCESS

STAR★METHODS

KEY RESOURCES TABLE

REAGENT or RESOURCE	SOURCE	IDENTIFIER
Deposited data		
MSEG/MEG and EMG data, dataset 1	This paper	Zenodo: https://zenodo.org/records/20824565 [DOI 10.5281/zenodo.20824565]
MSEG/MEG and EMG data, dataset 2	This paper	Zenodo: https://zenodo.org/records/20824827 [DOI 10.5281/zenodo.20824827]
Software and algorithms		
MATLAB R2021b	MathWorks	RRID: SCR_001622
Statistical Parametric Mapping (SPM), development version	Tierney et al.[52]	https://github.com/spm; RRID: SCR_007037
FieldTrip	Oostenveld et al.[53]	RRID: SCR_004849
NeuroSpec	Halliday[54]	https://github.com/dmhalliday/NeuroSpec
TotalSpineSeg	Warszawer et al.[55]	https://github.com/neuropoly/totalspineseg
ECGSim thoracic meshes	Van Oosterom and Oostendorp[56]	https://www.ecgsim.org
Custom analysis code	This paper	https://github.com/meaghanspedden/brainspine-connectivity; [DOI 10.5281/zenodo.21526103]
Other		
QuSpin Neuro-1 triaxial OPM system	QuSpin Inc.	N/A
Custom 3D-printed scanner-cast	Chalk Studios	N/A
EMG amplifier (BrainAmp series)	Brain Products	N/A
1401 data acquisition unit	Cambridge Electronic Design	N/A

EXPERIMENTAL MODEL AND STUDY PARTICIPANT DETAILS

Human participants

We recruited ten healthy, right-handed participants to take part in this series of experiments (6 female/4 male, self-reported sex; age range 20-58 years), and they provided written, informed consent. The study procedures were approved by the University College London Research Ethics Committee, and experiments were conducted in accordance with the Declaration of Helsinki. A fixed scanner-cast geometry (see Scanner-cast below) was optimized for one participant of the cohort but was used by all. One participant's data were excluded due to the failure of a reference OPM during the recording. For two participants, the head component of the scanner-cast either did not close properly or was too large, positioning the sensors too far from the scalp. As a result, brain analyses include n = 7, whereas spinal cord analyses include n = 9 participants. While the number of participants was limited due to the intensive nature of these recordings, each participant provided a large quantity of continuous data (~10 minutes of rest and 10 minutes of contraction per participant), facilitating in-depth single-participant analysis and group-level summaries.

Participants were healthy adults. Sex and age are reported above. Gender was not recorded separately from sex, and ancestry, race, ethnicity, and socioeconomic status were not collected, as this study was a methodological feasibility demonstration in a small sample in which these variables were not analytic factors. For the same reason, the influence of sex on the reported measures was not analyzed. The absence of these variables and analyses means that the findings should not be assumed to generalize across sex, gender, or demographically diverse populations.

METHOD DETAILS

OPM-based recording system

We developed an OPM-based system capable of performing concurrent recordings of brain and spinal cord activity while participants lay supine.

Please cite this article in press as: Spedden et al., Coherent oscillations across the human brain, spinal cord, and muscle network, Current Biology (2026), https://doi.org/10.1016/j.cub.2026.07.070

OPM acquisition

The QuSpin Neuro-1 acquisition system with third generation triaxial OPM sensors (QuSpin Inc., Louisville, CO, USA) was used to record OPM data. The sensors have an intrinsic bandwidth of 0-135 Hz due to the properties of the vapour cell, in addition to a low-pass 6th order Chebyshev Infinite Impulse Response filter at 150 Hz.

Experiments were conducted in a magnetically shielded room (MSR) (438 x 338 x 218 cm; Magnetic Shields Ltd, Staplehurst, UK). The inner layer of mu metal lining the room was degaussed using a low-frequency decaying sinusoid driven through cables within the walls prior to the start of the experiment. The OPM sensors were then nulled using on-board nulling coils and calibrated.

Scanner-cast

Sensors were positioned in a custom-built, 3D-printed rigid nylon scanner-cast (Chalk Studios, London, UK) to record brain and spinal cord activity. The cast was designed from a negative mold of Participant 1's head, neck, and back. The scanner-cast includes sensor slots covering the scalp, neck, chest, and back (Figure 1A). During recording, the cast was positioned in order to keep the participant at a height near the center of the room where the background field is most effectively nulled.

For the remaining eight participants, the torso component of the scanner cast fit well, such that it could be closed completely and the back and neck rested flush against the surface. As a result of the participant-specific construction, Participant 1 represents an optimal recording case with the most precise sensor-to-anatomy correspondence. Single-participant results from Participant 1 are presented alongside group-level analyses throughout, to illustrate the clarity of effects achievable under ideal recording conditions and to assess robustness across participants.

EMG recordings

EMG was recorded from the right abductor pollicis brevis muscle (APB) using pairs of surface electrodes (Ambu Ltd, Ballerup, Denmark). The APB is innervated by the median nerve, which enters the spinal cord around C8-T1.[57] The reference electrode was fastened around the right wrist. To prevent EMG data collection from interfering with OPM acquisition, EMG signals were amplified and digitized outside the MSR (BrainAmp series, Brain Products, Gilching, Germany). To achieve this, EMG cables were passed through waveguides in the MSR. EMG and OPM data were synchronized based on a TTL pulse sent from a 1401 data acquisition unit (Cambridge Electronic Design; Cambridge, UK) to the EMG and OPM acquisition systems.

Task

During recordings, participants lay supine in the MSR with their back and neck resting in the scanner-cast (Figure 1A).

We selected a weak, sustained contraction of a distal muscle as our task because it is consistently reported to elicit corticomuscular coherence,[28,58,59] providing a useful point of departure for further investigating functional connectivity between the brain, spinal cord, and muscle. Participants were asked to maintain a weak thumb abduction (instructed as $\sim$ 15 % of maximal voluntary contraction) and given a small object to hold for resistance. We alternated between two minutes of right thumb contraction and two minutes of rest, and each participant completed five cycles of the two conditions. EMG activity was monitored online to ensure that contraction intensity remained relatively stable. Real-time visual feedback of the EMG signal could not be provided to participants due to hardware limitations of the amplifier used for EMG recording; instead, the experimenter verbally instructed participants to slightly increase or decrease their contraction strength if the monitored EMG level appeared to drift noticeably from the level established at the start of the contraction block.

Data analysis software

All data analysis was performed in MATLAB R2021b (Mathworks Inc., Natick, MA, USA) using the development version of Statistical Parametric Mapping (SPM; https://github.com/spm)[52] and the Fieldtrip[53] toolbox.

Preprocessing of OPM and EMG data

In the following, we use the terms 'sensor' to describe one triaxial OPM sensor and 'channel' to describe the signal from one sensor axis. OPM data were imported into SPM and power spectra were inspected for evidence of bad channels, i.e., channels exhibiting large deviations from the median power spectrum and the manufacturer's noise floor, which were removed from the data set.

First-order homogeneous field correction (HFC) was applied to brain and spinal cord data for interference suppression. HFC models the interference as a spatially constant field and can reduce environmental noise over a broad range of frequencies.[60] OPM and EMG data were high pass filtered with a cutoff frequency of 5 Hz, then low pass filtered with a cutoff frequency of 45 Hz, using 5th order Butterworth filters, then 3rd order band stop filters from 48-52 and 98-102 Hz were applied.

After filtering the OPM data, large heartbeat artefacts were apparent on most channels. We removed these artefacts using signal space projection (SSP).[61] We used a channel from an OPM sensor positioned above the heart to identify the timing of cardiac R-peaks, reflecting the heartbeat artefact time course. These R-peaks were then used to epoch the OPM data from all channels, and an artefact template was constructed by averaging the epoched data time-locked to the main peak of the cardiac artefact. Data were then downsampled to 1000 Hz to match the EMG sampling frequency, and the EMG and OPM data were synchronized based on the TTL pulse.

Using one reference sensor positioned on the support structure for the scanner-cast, i.e., away from the participant (approximately 15 cm above and 20 cm lateral to the participant's inion), we then performed synthetic gradiometry,[62] regressing data from the

Please cite this article in press as: Spedden et al., Coherent oscillations across the human brain, spinal cord, and muscle network, Current Biology (2026), https://doi.org/10.1016/j.cub.2026.07.070

reference sensor out of the brain and spinal cord channels. The reference sensors capture environmental interference, but not neural signals; consequently, the synthetic gradiometry subtracts this interference from the signals of interest.

Data were then segmented into non-overlapping epochs with one second duration. Trials were classified as outliers using a threshold of 3 median absolute deviations (MADs) above the median mean trial standard deviation. Outlier trials were removed, and remaining trials were concatenated across runs. Finally, data were projected using SSP into a subspace orthogonal to the heartbeat artefact direction. Note that the projector was constructed from both rest and contraction conditions and that lead fields were pre-multiplied by the HFC and SSP projectors[61] to account for any distortions induced by the projectors in the signal. The EMG signal was rectified for coherence analysis.[63]

Co-registration and forward models

Structural MRI data were acquired on a 3T Siemens Prisma system using a combined head-spine setup (spoiled gradient echo, isotropic resolution = 1.5 mm, TE = 2.10 ms, TR = 5.85 ms, flip angle = 6°). A 24-channel spine coil array was placed directly beneath the scanner-cast, while a 64-channel head and neck coil covered the cranial region. To image the full extent of interest, from the cranial base to the lower thoracic spine, multiple consecutive acquisitions were obtained along the cranial-caudal axis. Given the large field of view of each acquisition, gradient non-linearity correction was applied. The MRI data were used to segment the spinal cord and vertebral column[55,64] (https://github.com/neuropoly/totalspineseg) and to define a column of source points along the spinal cord of Participant 1 at 5 mm resolution, extending through the region covered by the sensors.

Co-registration of OPM sensor positions to anatomy was achieved by creating a rigid mold of Participant 1's back shape in the supine position and using this to construct (1) the OPM scanner cast and (2) an MRI compatible scanner-cast; this ensured that the participant was positioned identically during functional and structural scanning sessions. We also performed a 3D optical scan (Einscan, Shining 3D; Hangzhou, China) of Participant 1 lying in the MRI cast to obtain a complete 3D representation of the upper body in the supine position.

Spinal cord magnetic field forward modelling was performed using a Biot-Savart law approximation, following the approach of Kawabata and colleagues.[14] Each source point was modelled as a current dipole oriented along three orthogonal axes along the center line of the spinal cord, with the magnetic field at each sensor computed analytically from the sensor-source geometry. Because the scanner-cast fixes sensor positions identically across participants, a single leadfield matrix could be applied consistently to all nine participants using the same reference source space.

In our forward model for the brain, we used the canonical brain mesh from SPM, transformed into Participant 1's native space using the Procrustes and ICP method with nasion, left pre-auricular point, and right pre-auricular point as fiducials. The mesh volume was filled with a regular grid of source points (spacing 5 mm) and modelled using a single-shell volume conductor.[65] Leadfields were computed using FieldTrip, modelling each source with three orthogonal orientations.

These anatomical models were used as a common reference for forward modelling in all participants, reflecting the fixed geometry of the scanner cast.

Source localization of coherent activity

Using beamforming analysis we sought to quantify (1) brain-EMG coherence; and (2) spinal cord-EMG coherence.

Using these forward models, we first sought to identify brain and spinal cord sources exhibiting coherence with the EMG signal measured from the APB. We applied Dynamic Imaging of Coherent Sources (DICS) beamforming[66] in FieldTrip to OPM data from contraction and rest conditions, using the EMG as a reference channel.

Virtual electrode time series were subsequently extracted at the peak coherence locations identified by DICS, and coherence spectra between all three signal pairs (motor cortex, spinal cord, and muscle EMG) were computed to characterize the frequency profile of cortico-spinal-muscular coupling (see 'Virtual Electrodes' below).

Coherence was computed within the 10-35 Hz range, chosen to encompass mu and beta frequencies known to show strong movement-related modulations in the cortex.[27] Cross-spectral density (CSD) matrices were estimated for all spinal cord and brain OPM channels and the EMG signal within this frequency band. Beamformer weights were computed using a common spatial filter derived from a pooled CSD matrix across both contraction and rest conditions. Tikhonov regularization ($\lambda = 10\%$) was applied to stabilize the inversion. Each source location was modelled with three orthogonal orientations, and the orientation was set to that which maximized projected source power.

Prior to statistical inference, source coherence maps were spatially smoothed using a Gaussian kernel (brain: FWHM = 8 mm; spinal cord: FWHM = 20 mm). The larger kernel applied to spinal cord maps reflects the expected variation in the region of interest (over participants) and the use of a common anatomical reference rather than individual participant anatomy.

This yielded source-level estimates of coherence with EMG for both contraction and rest conditions in the brain and spinal cord for each participant. Differences between conditions were assessed using permutation testing (500 label permutations; see quantification and statistical analysis).

Spinal cord source geometry

To further characterize the spinal cord signal identified using spinal cord-EMG coherence, we examined the dominant source orientation at the peak source location. For each permutation, the source with the maximum coherence difference was identified, and its spatial filter ($3 \times n$ channels) was decomposed using singular value decomposition. The dominant orientation was defined as the first

Please cite this article in press as: Spedden et al., Coherent oscillations across the human brain, spinal cord, and muscle network, Current Biology (2026), https://doi.org/10.1016/j.cub.2026.07.070

left singular vector, representing the direction of maximum projected power. The dominant axis was labelled according to the component with the largest absolute value.

Spatial specificity of the spinal source

To determine whether the spinal source location and orientation identified by the spinal cord-EMG analysis reflected a genuine task-related effect rather than a systematic bias of the source reconstruction procedure, we examined the spatial and orientational distribution of peak coherence differences obtained under permutation. For Participant 1, the source location and dipole orientation corresponding to the maximal coherence difference (contraction-rest) were extracted for each of 500 label permutations. The resulting null distribution of peak locations and orientations was visualized to assess whether the observed source estimate occupied a position or alignment that was preferentially selected under permutation.

Virtual electrodes

To further characterize interactions within the identified cortico-spinal-muscle network, virtual electrodes were defined in the spinal cord and brain source spaces.

The spinal cord virtual electrode was defined based on the spinal cord-EMG results and principal component projection of the reconstructed time series within the region exhibiting the largest contiguous cluster of coherence with EMG. The resulting principal component served as the representative spinal cord signal for each participant.

A brain virtual electrode was reconstructed for each participant by intersecting two constraints: a spherical region of interest centered on the primary motor cortex (MNI coordinate [−38, −26, 56], radius 20 mm), and the primary sensorimotor hand area cluster identified in the brain-EMG coherence prevalence map. Source reconstruction was performed using the previously described beamforming framework, and the reconstructed time series from this region served as the brain virtual electrode for subsequent analyses.

Coherence, directionality, and dynamics

To investigate the directionality and dynamics of interactions within the identified cortico-spinal network, we examined three signals for each participant: the brain virtual electrode, the spinal cord virtual electrode, and the EMG signal.

We used NeuroSpec (https://github.com/dmhalliday/NeuroSpec)[54,67] to compute coherence spectra for each signal pair and participant using the multitaper method.[68] To assess the statistical significance of brain-spinal cord coherence, we applied the upper confidence limit on coherence under the null hypothesis of zero true coupling given by $1 - \hat{\alpha}(1/(L - 1))$,[69] where L is the number of independent segments contributing to the spectral estimate and $\alpha = 0.05$.

Frequency-domain directionality was quantified using nonparametric directed coherence as implemented in NeuroSpec. Directed coherence was computed from the factorization of the cross-spectral density matrix and provides a frequency-specific estimate of the direction of coupling between each pair of signals without assuming a parametric model. To evaluate the robustness of the directed coherence estimates we additionally computed the phase slope index (PSI), which quantifies the consistency of the direction of change in the phase difference spectrum over frequencies weighted by the coherence.[70]

To characterize temporal dynamics, we used the normalized cumulant density (ρ), a time-domain measure equivalent to the whitened cross-correlation function.[54] The ρ function estimates time-lagged coupling and identifies the delay at which activity in one signal best predicts the other. For each participant, peak latencies were identified as the lag corresponding to the maximum $|\rho|$ within a ±50 ms window. To mitigate the influence of instantaneous shared noise or field spread, which can produce spurious near-zero coupling, lags within ±2 ms of zero were excluded. Peak latencies were therefore defined as the maximum $|\rho|$ occurring in the window of interest and were used to summarize the timing of interactions across participants.

Spectral power

We then wanted to determine whether the neural coherence could be explained by changes in signal amplitude, so we performed a control analysis of spectral power in the 10-35 Hz band. Spectral power was estimated from the brain and spinal cord virtual electrodes for each participant using the same time window and preprocessing as for the coherence analysis. Power values were averaged across the 10-35 Hz band and log-transformed prior to statistical testing to stabilize variance. Band power was compared between contraction and rest trials using a paired t-test, applied both at the individual level (Participant 1) and at the group level across participants with both brain and spinal cord data (n = 7).

To further isolate oscillatory power from the underlying aperiodic component of the spectrum, we additionally applied the FOOOF (Fitting Oscillations and One Over f) algorithm[71] to each power spectrum. This approach parametrizes the power spectrum as the sum of an aperiodic component, characterized by a broadband offset and exponent, and periodic components, modelled as Gaussian peaks. We then extracted the periodic component and repeated the comparison between contraction and rest on this aperiodic-corrected signal using the same paired t-test procedure at the group level (n = 7).

Forward model sensitivity analysis

To quantify the sensitivity of the forward model to inter-participant variability in sensor placement, we simulated the effect of sensor displacement on the Biot-Savart leadfield by shifting the entire sensor array by random displacement vectors drawn from three magnitude bands: small (2.83-4.19 mm, mean 3.41 ± 0.40 mm), medium (7.88-9.39 mm, mean 8.81 ± 0.49 mm), and large (14.22-20.15 mm, mean 17.86 ± 2.09 mm), with 8 random directions sampled per band (24 conditions total). Within each band, shift

Please cite this article in press as: Spedden et al., Coherent oscillations across the human brain, spinal cord, and muscle network, Current Biology (2026), https://doi.org/10.1016/j.cub.2026.07.070

directions were distributed across all three axes with no preferred orientation, ensuring coverage of realistic co-registration error scenarios.

For each shifted condition, sensitivity was quantified by computing, for each source point along the cord, the R^2 of the correlation between the original and shifted leadfield columns across all sensors. We focused on the dipole orientation that was most prevalent in the data, ventral-dorsal. For display, three representative conditions spanning the sampled range are shown (4.2, 15.7, and 20.1 mm).

Inter-participant positional variability was estimated by measuring the displacement of each participant's C7 vertebra relative to a fixed landmark on the cast, yielding a range of ±15 mm (n = 7; measurements were obtained post hoc from the participants who could be re-contacted). The displacement magnitudes shown in Figure S4 were selected to span this range, with the largest (20.1 mm) exceeding it.

To assess the downstream effect on coherence localization, the spinal cord-EMG DICS analysis was rerun for Participant 1 using a representative shifted leadfield (17.9 mm) randomly selected from the large bundle, with all other analysis parameters held constant. Peak coherence location and the spatial profile of statistical significance were compared between the original and shifted solutions.

Boundary element model comparison

The spinal cord source localization pipeline described in the main text uses a Biot-Savart approximation to compute the leadfields for spinal cord sources. An anatomically detailed boundary element model (BEM) is in ongoing development in parallel.[48,49] For perspective, we summarize both models here and compare their outputs.

The BEM was constructed from a brain-to-whole-spine T_1-weighted MRI acquired at 3T (1.5 mm isotropic resolution. Briefly, the outer torso, vertebral column, and spinal cord were segmented using TotalSpineSeg[55] and thoracic organ meshes (heart, lungs) were incorporated from ECGSim[56] and co-registered via a 7-DOF Procrustes followed by 12-DOF affine ICP refinement. All meshes were scaled to a participant-specific optical surface scan captured in a custom scanner-cast to preserve supine geometry across MRI and OPM environments.[49]

First, we compared the localization of spinal cord-EMG coherence using the Biot-Savart and BEM forward models using the same pipeline described in the main manuscript. The Biot-Savart solution localises peak coherence to the mid-cervical region consistent with the expected innervation level for upper-limb hand muscles (centred roughly on C7). The BEM solution yields a broadly comparable result but shifted slightly caudally (centred roughly on T2) relative to the Biot-Savart model (Figures S4D and S4E).

Second, we assessed the sensitivity of the BEM leadfields to sensor position uncertainty using the same approach applied to the Biot-Savart model, computing the R^2 between the nominal sensor array leadfield and leadfields computed at simulated array positions representative of between-participant variability in sensor-to-body geometry (Figure S4B).

Partial coherence and peak frequency

To assess whether brain-EMG coherence could be explained by signal passing linearly through the spinal cord, we recomputed brain-EMG coherence after partialling out the spinal cord signal. Partial coherence was estimated using a multitaper approach (DPSS tapers; time-bandwidth product NW = 4), with the spinal cord virtual electrode signal regressed out of both the brain and EMG signals in the frequency domain at each frequency bin before recomputing coherence between the residuals. For each participant, the peak in full (non-partialled) brain-EMG coherence within the 10-35 Hz analysis band was identified, and the partial coherence value at that same frequency bin was extracted for comparison. The percent reduction in coherence at this frequency was calculated for each participant and tested against zero across the group using a Wilcoxon signed-rank test.

As a complementary analysis, we tested whether the three coherence pairs (brain-EMG, brain-spinal cord, spinal cord-EMG) shared a common peak frequency within the 10-35 Hz band. For each participant, the frequency at which coherence peaked was identified separately for each pair, and peak frequencies were compared pairwise across the group using paired t-tests (brain-EMG vs. brain-spinal cord; brain-EMG vs. spinal cord-EMG; brain-spinal cord vs. spinal cord-EMG). Here, the paired t-test asks whether the two signal pairs share a common peak frequency at the group level.

QUANTIFICATION AND STATISTICAL ANALYSIS

To assess whether coherence differed between contraction and rest conditions, statistical inference was performed at both the single-participant and population levels.

Single-participant inference

For each participant, statistical significance of coherence differences (contraction > rest) was assessed using permutation testing (n = 500). Condition labels were randomly shuffled at each iteration, and the maximal coherence difference across all source locations was retained to construct a null distribution.[72] Smoothing was applied to both the observed coherence difference map and each permutation sample prior to thresholding. Multiple comparisons were controlled using a max-statistic approach: the 95th percentile of the maximal permuted values served as the global significance threshold. Observed coherence differences exceeding this threshold were considered statistically significant. This yielded, for each participant, a spatial map of significant coherence differences relative to a within-participant null distribution.

Please cite this article in press as: Spedden et al., Coherent oscillations across the human brain, spinal cord, and muscle network, Current Biology (2026), https://doi.org/10.1016/j.cub.2026.07.070

Population prevalence inference

To assess the robustness of coherent effects across participants, we treated each participant as an independent replication. For each participant, we determined whether at least one brain or spinal cord source exhibited statistically significant coherence relative to the within-participant null distribution, yielding a binary outcome per participant (presence or absence of a significant coherent effect).

We then estimated the population prevalence of the effect using Bayesian prevalence inference.[37] This approach models the proportion of the population expected to show a true effect, given the number of significant participants, the sample size, and the false-positive rate of the single-participant test. We report the maximum a posteriori (MAP) estimate of prevalence together with highest posterior density intervals (HPDIs), providing an estimate of the proportion of the population exhibiting coherent effects.

For illustration, significant coherence differences (contraction > rest) were visualised using -log10(p) values for Participant 1 interpolated on the brain and spinal cord meshes.

Prevalence maps summarised the fraction of participants showing significant coherence at each source location. This approach is conceptually similar to conjunction analyses[73] in which participants are treated as independent replications to assess robustness of effects rather than to support conventional random-effects spatial inference. In this context, significant effects in anatomically plausible brain and spinal cord regions are informative despite the reduced spatial precision inherent to the group analysis.

Reporting of statistical parameters

Statistical parameters, including the exact value of n, what n represents, dispersion measures, and the criteria for significance, are reported in the Results, the figure legends, and the subsections above. Most comparisons used non-parametric permutation and rank-based tests, which do not require distributional assumptions. Paired t-tests were used for the comparisons of spectral power described in the method details. Normality was not formally assessed, given the sample size.